Mo isotopic composition of the mid-Neoproterozoic ocean: an iron formation perspective

Geoffrey J. Baldwin[1]*, Thomas F. Nägler[2], Nicolas D. Greber[2], Elizabeth C. Turner[1], and Balz S. Kamber[3]

[1]Department of Earth Sciences, Laurentian University, Sudbury, ON, Canada P3E 2C6

[2]Institut für Geologie, Universität Bern, Baltzerstr. 1, 3012 Bern, Switzerland

[3]Department of Geology, Trinity College Dublin, Dublin 2, Ireland

*Corresponding author

geoff.j.baldwin@gmail.com

Keywords: Mo isotopes; Rhenium; Neoproterozoic; iron formation

Abstract

The Neoproterozoic was a major turning point in Earth's surficial history, recording several widespread glaciations, the first appearance of complex metazoan life, and a major increase in atmospheric oxygen. Marine redox proxies have resulted in many different estimates of both the timing and magnitude of the increase in free oxygen, although the consensus has been that it occurred following the Marinoan glaciation, the second globally recorded "snowball Earth" event. A critically understudied rock type of the Neoproterozoic is iron formation associated with the Sturtian (first) glaciation. Samples from the <716 Ma Rapitan iron formation were analysed for their Re concentrations and Mo isotopic composition to refine the redox history of its depositional basin. Rhenium concentrations and Re/Mo ratios are consistently low throughout the bottom and middle of the iron formation, reflecting ferruginous to oxic basinal conditions, but samples from the uppermost jasper layers of the iron formation show significantly higher Re concentrations and Re/Mo ratios, indicating that iron formation deposition was terminated by a shift towards a sulfidic water column. Similarly, the δ^{98}Mo values are close to 0.0‰ throughout most of the iron formation, but rise to ~+0.7‰ near the top of the section. The δ^{98}Mo from samples of ferruginous to oxic basinal conditions are the product of adsorption to hematite, indicating that the Neoproterozoic open ocean may have had a δ^{98}Mo of ~1.8‰. Together with the now well-established lack of a positive Eu anomaly in Neoproterozoic iron formations, these results suggest that the ocean was predominantly oxygenated at 700 Ma.

Research Highlights

- Samples from the Rapitan iron formation were analysed for Re and δ^{98}Mo. Both proxies record sulfidic conditions at the top of the iron formation. δ^{98}Mo records the interplay between sulfidic waters and adsorption to hematite. The mid-Neoproterozoic ocean had a δ^{98}Mo only slightly lower than that of the modern ocean.

1. Introduction

The Neoproterozoic was a critical time in the Earth's surficial evolution. It witnessed the global "snowball Earth" glaciations (Kirschvink, 1992) and the subsequent appearance of the first complex metazoan life (e.g., Canfield et al., 2007). One of the most significant developments in the Neoproterozoic was a major rise in atmospheric oxygen content and the apparently concomitant increase in marine oxygenation (Och and Sheilds-Zhou, 2012). This ventilation of the ocean represents a major change from conditions earlier in the Proterozoic. Following the Great Oxygenation Event (GOE) between 2.4 and 2.3 Ga (Bekker et al., 2004), the ocean apparently remained unoxygenated at depth throughout the Paleo- and Mesoproterozoic. The precise redox conditions of the deep open ocean during this time are subject to considerable debate, and it has been suggested that the global deep ocean was sulfidic during this time (Canfield, 1998). Studies using both iron speciation (e.g., Poulton et al., 2004; Shen et al., 2002) and molybdenum isotopes (Arnold et al., 2004) initially supported this interpretation. More recent work has shown, however, that the deep ocean was probably ferruginous or even locally oxic during this interval (e.g., Planavsky et al., 2011; Poulton et al., 2010; Slack et al., 2007), and remained so into the early to middle Neoproterozoic (e.g., Johnston et al., 2010), and perhaps into the Ediacaran (e.g., Canfield et al., 2008; Li et al., 2010). The growing consensus is that the Proterozoic water column was oxygenated at shallow depths, had ferruginous deep water, and contained limited, near-shelf, mid-depth sulfidic conditions around areas with high biological primary productivity and organic carbon burial (Poulton and Canfield, 2011).

The gradual redox evolution of the ocean is reflected by several geochemical proxies, including Mo concentrations in black shales (e.g., Scott et al., 2008), which show a distinct, three-step increase over time, corresponding to the GOE and the late Neoproterozoic rise in oxygen ("NOE"), respectively. This gradual increase in Mo content in black shale and the implied commensurate rise in seawater Mo was explained as the result of more widespread anoxic and sulfidic water masses in the ocean than prevail today. Accordingly, the Mo inventory of seawater was limited prior to the NOE by Mo fixation into sediment below sulfidic water masses (Scott et al., 2008). Due to this increased Mo fixation rate, it is generally assumed that the δ^{98}Mo composition of Proterozoic seawater would have been isotopically light, because

under high sulfide concentrations Mo is scavenged from ambient seawater without significant isotope fractionation (Neubert et al., 2008). This behaviour would result in Proterozoic seawater being ≥1.0‰ lighter than its modern counterpart, as has been observed in black shales of both Meso- (Arnold et al., 2004) and early Neoproterozoic age (Dahl et al., 2011). These interpretations rely on the assumption that the studied shales were deposited in basins with full connectivity to the open ocean and that other redox proxies can reliably distinguish between sulfidic, ferruginous, or oxic conditions. Their validity notwithstanding, these studies represent all but two data points covering a time interval in excess of one billion years, clearly indicating the need for further work in this area.

An additional, unusual attribute of the Neoproterozoic was the deposition of iron formation, which, with very few exceptions, had not occurred since the late Paleoproterozoic (Bekker et al., 2010). Although the ocean had apparently remained ferruginous throughout the Meso-and early Neoproterozoic, very little iron formation was deposited except during the <716 Ma Sturtian glaciation (Macdonald et al., 2010a; 2010b), with a few older (e.g., Slack et al., 2007) exceptions. Numerous models have been proposed to explain the causes for the return of iron formation, and the development of the widespread "snowball Earth" glacial events have been critical in the development of these models (e.g., Baldwin et al., 2012; Klein and Beukes, 1993). Equally important was the development of a complex water column redox stratigraphy, similar to that described by Poulton and Canfield (2011), which allowed for the build-up of significant dissolved iron in basins that deposited iron formations (Baldwin et al., 2012).

The least understood aspect of Sturtian iron formation is its apparently abrupt termination. Did a sudden influx of clastic detritus overwhelm deposition of hydrogenous sediment, or did water column chemistry change sufficiently to make the iron deposition impossible? Using trends in authigenic Mo enrichment, Baldwin et al. (2012) proposed that the water column was becoming more sulfidic towards the end of iron formation deposition, which eventually stopped the oxidation of dissolved ferrous iron to ferric iron oxy-hydroxides. This proposal was built on the elemental Mo proxy only. In the present study we set out to test this hypothesis more rigorously. Using jasper samples from the Rapitan iron formation, north-western Canada (Fig. 1A) that have already been characterised according to their sedimentology

and their rare earth element (REE+Y), Mo, and U chemistry, we present δ^{98}Mo and Re elemental data to elucidate the causes of the termination of iron formation deposition and provide insight into the δ^{98}Mo composition of middle Neoproterozoic seawater.

2. Sampling and analytical methods

2.1 Stratigraphy and sample selection

A continuous stratigraphic section through the Neoproterozoic Rapitan iron formation, Northwest Territories, Canada (Fig. 1A), was documented at centimetre-scale. Previously described by Baldwin et al. (2012), the iron formation at this location is 35 m thick, and is underlain by purple hematite- and clast-rich diamictite with localised channels of clast-supported tan polymictic conglomerate (Fig. 3). The iron formation is of the oxide-facies type, with the iron mineralogy consisting of jasper and hematite, and accessory calcite and dolomite present in small but variable abundances. Texturally, the iron formation is characterised by interbedded jasper and massive hematite beds, or banded iron formation (BIF), and is in nearly equal proportion to intervals of massive hematite with zoned, lensoidal jasper nodules 0.5-50 cm in diameter. Glacially derived dropstones are common throughout the iron formation, occurring in such high concentrations at several horizons as to constitute a hematite-matrix diamictite. Thin siliciclastic intervals of siltstone and polymictic conglomerate are also present (5-40 cm thick). The iron formation is sharply overlain by tan to grey, clast-poor diamictite (Fig.1B, C), which contains a thin interval of hematite-bearing diamictite consisting of reworked iron formation clasts several metres above the uppermost intact iron formation layer (Fig. 1B). Textual evidence from dropstones indicates that, at a minimum, partial lithification occurred fairly early: even large dropstones (up to 15 cm) penetrate bedding by only a maximum of half the diameter of the dropstone (Fig. 2A). Similarly, textural evidence from hematite microbands shows that in addition to fairly early compaction and partial lithification, any primary iron mineralogy was converted to hematite very early in the diagenetic process, with bands at the sub-millimetre scale preserved both in outcrop (Fig. 2B) and at the microscopic scale (Fig. 2C).

126 Sampling focussed on jasper beds as opposed to nodular iron formation, for reasons
127 explained in Baldwin et al. (2012). Jasper beds were mechanically separated from associated
128 hematite beds, and all samples reported here are from jasper beds in the iron formation interval.

129 2.2 Digestion and trace element analysis

130 In view of the anticipated low Mo and Re concentrations, special care was taken to test
131 reagents for blank levels prior to the analyses. The main source of blank was found to be HF, and
132 for this reason, a dedicated batch of HF was produced by sub-boiling 5-fold distillation. The total
133 procedural blank for Mo trace element analysis (i.e., digestion, dilution, and analysis) was
134 determined in duplicate, and yielded 0.100 and 0.093 ng, respectively. Trace elements other than
135 Re were determined by solution ICP-MS, and Mo analysis was calibrated with a dedicated
136 standard-addition experiment (Baldwin et al., 2012). The accuracy of the Mo data was tested by
137 comparison with data obtained by isotope dilution (see section 2.3) and was found to be excellent
138 (Suppl. Fig. 1). Analyses took advantage of the high Si content (typically >65 wt%) of the
139 samples, which results in low matrix load of the final solution (due to loss of Si as SiF_4). This
140 afforded very low detection limits, as explained in Baldwin et al. (2011).

141 2.3 Rhenium

142 Sample stock solutions from trace element analysis of jasper samples used in Baldwin et
143 al. (2012) were spiked with 20 pg of enriched ^{185}Re. The spiked solutions underwent a modified
144 column separation chemistry after Fischer-Gödde et al. (2011) to remove elemental matrix for Re
145 analysis. The purified Re solutions were analysed for isotope composition by isotope dilution
146 inductively-coupled plasma mass spectrometry (ID-ICP-MS) on a Thermo X series II quadrupole
147 ICP-MS at Laurentian University. Mass bias was estimated using the standard-sample-standard
148 bracketing technique. Full errors in weights, spike composition, mass bias, and analysis were
149 propagated (1-σ).

150 For the lowest-concentration samples the largest sources of uncertainty were the blank
151 contribution (determined in triplicate to be 0.18±0.04 pg) and over-spiking. In the very lowest
152 concentration samples, the blank contributed up to 40% of the total Re. The samples were spiked
153 with 20 pg of ^{185}Re from an anticipated 800:1 mass ratio of Mo:Re, derived from exploratory

laser ablation ICP-MS (LA-ICP-MS) analysis of samples from the uppermost iron formation strata. These samples proved to be the ones with the lowest Mo:Re. Regardless of the large relative errors on the single-digit ppt data, the critical aspect of the data was that the majority of samples have exceedingly low Re contents. Rhenium concentrations were calculated based on the known natural isotopic abundances of ^{185}Re and ^{187}Re, and the recorded mass of added ^{185}Re.

Accuracy of the method was tested by analyses of the rock reference materials BHVO-1, BCR-2, and Sco-1. The Re concentrations obtained for these materials are slightly higher (6.5% for Sco-1, 6% for BHVO-2 and 19% for BCR-2) than those published by Meisel and Moser (2004), who did not digest with HF. According to Meisel et al. (2009), this outcome is because HF digests release Re held in silicates (e.g., clinopyroxene in the basaltic reference materials BHVO-1 and BCR-2).

2.4 Mo isotopes

The Mo-isotope data were obtained on aliquots of the same powder used for the trace element analysis. This had been carefully obtained from thin slices adjacent to thin sections. Between 0.63 and 1.44 g of powder aliquot was digested with a 4:1 mixture of 5-fold distilled HF and 3-fold distilled HNO_3. The resulting solution was then spiked and split in two to allow for duplicate analyses. A ^{100}Mo-^{97}Mo double spike was used to enable corrections for mass biases produced during chemical separation and MC-ICP-MS measurement. The use of a double-spike allows for the simultaneous determination of the Mo isotope composition and the Mo concentration using isotope dilution. The Mo concentration can be determined to a precision of ±2% (Greber et al. 2012). Molybdenum was separated from the sample matrix using a sequential procedure involving anion and cation exchange chromatography, as described in Wille et al. (2007). The anion chromatography was employed twice, to ensure total Fe removal. For each chemical separation step, 3x-distilled HCl and HNO_3 were used, resulting in a procedural blank of $\leq$ 1.5 ng Mo.

The $\delta^{98}Mo$ composition of all samples were analysed using a double-focussing Nu Instruments ^{TM} MC-ICP-MS system (Wrexham, Wales, UK). Measurement procedure and double-spike calibration are described in Greber et al.(2012), employing the double-spike

mathematics outlined in Siebert et al. (2001). The precision under intermediate-precision conditions is better than ±0.1‰ (2SD) for both liquid standards (see below) and the NIST SRM 610 and 612 glasses (see Table 1 and Greber et al. 2012). A Johnson Matthey ICP standard solution (lot 602332B) was used as reference material. Its δ^{98}Mo composition is 0.25‰ lower than the NIST SRM 3134 and 2.34‰ lower than the mean open ocean water Mo (Greber et al. 2012).

3. Results

3.1 Rhenium

Rhenium concentrations range from 2.3 to 358 parts per trillion (ppt), with a mean value of 39.8 ppt, and a median of 9.7 ppt, reflecting a strong bias in the dataset towards low concentrations. Eleven out of 22 samples have low concentrations of Re, with less than 10 ppt, whereas eight others have concentrations in the double-digit ppt. Only three samples contain >100 ppt Re, all from the top of the stratigraphic section, and all leaving reduced carbon stains in the digestion beakers. Single-digit Re concentrations are distributed throughout the section, whereas double-digit values are restricted to the bottom and middle of the succession. Recorded Re/Mo ratios, an extremely sensitive indicator of marine redox conditions (e.g., Crusius et al., 1996; Morford et al., 2005; Nameroff et al., 2002), ranged from 6.49×10^{-6} to 1.02×10^{-3} (ppb/ppb), with mean values of 1.93×10^{-4}. Eighteen of 22 samples have Re/Mo ratios well below the average modern seawater ratio of 8.0×10^{-4} (Pattan and Pearce, 2009), whereas two of the three samples from the top of the section show higher Re/Mo ratios than modern seawater (Fig. 3).

Rhenium has a very low crustal abundance, and is rendered completely soluble during oxidative weathering, thus minimizing its detrital flux to the marine realm. Consequently, absolute concentrations can be used as a redox proxy in most sedimentary rock types without significant influence of detritally sourced Re. In clean hydrogenous sediment such as jasper, with very low Al content, the clastic mineral contribution to the total Re inventory is negligible. In the present dataset, there is no correlation between Re concentration and common clastic indicators such as Al, Sc, or Th. Under oxic marine conditions, Re is present as the highly soluble

perrhenate ion (ReO_4^-), but Re becomes reduced and more insoluble at oxygen levels just below the oxygen level at which U and Fe reduction take place, and well before the appearance of free H_2S (Morford and Emerson, 1999). In this context, the limited fixation rate throughout most of the iron formation implies predominantly oxic conditions. The appearance of significantly higher Re concentrations at the top of the section, however, records a pronounced shift towards increasingly anoxic conditions. This shift is also recorded by elevated Re/Mo ratios in the same samples. Typically, Re/Mo ratios well below those of modern seawater record oxic conditions, despite very low, depleted concentrations of both elements. This is due to the comparatively high (but absolutely very low) fixation rate of Mo through adsorption to Fe and Mn oxy-hydroxides in comparison to Re, which is unaffected by Fe and Mn cycling (Crusius et al., 1996; Morford and Emerson, 1999). Sedimentary Re/Mo ratios significantly greater than that of modern seawater, in turn, record suboxic to anoxic conditions due to strong Re fixation relative to Mo. Seawater-like ratios record sulfidic conditions due to strong fixation of both Re and Mo, thus preserving the ambient metal budget (Crusius et al., 1996). Samples from the top of the iron formation alternate between greater than and less than the modern seawater ratio, but clearly remain close to that value. This result suggests that, at the top of the section, the marine redox conditions were becoming increasingly anoxic, and possibly mildly sulfidic.

3.2 Mo isotopes

Molybdenum isotopic data, expressed as δ^{98}Mo, range from -0.22 to +0.71‰, with errors in the range of 0.03-0.10‰. Throughout most of the stratigraphic section, δ^{98}Mo is at approximately crustal (0.0‰) to slightly negative values. One sample at 13.6 m is fractionated towards heavier δ^{98}Mo, with a value of 0.37‰ ±0.10‰, but overlying samples show fractionation levels similar to those seen in lower strata. The uppermost three samples all have a significantly heavier Mo isotope signature, with δ^{98}Mo values of 0.51, 0.71, and 0.70‰.

Crustal δ^{98}Mo is approximately 0.0‰ (e.g., Barling et al., 2001), with crustal igneous rocks generally between -0.1‰ to +0.3‰ (Siebert et al., 2003). Published δ^{98}Mo values of crustal MoS_2 vary widely over a few per mil, but the average δ^{98}Mo value is ~0.4‰ (Greber et

al., 2011). Modern open ocean water is homogeneous within <±0.2‰ (2 SD), irrespective of ocean or water depth (e.g., Nakagawa et al., 2012; Siebert et al., 2003). Apparent variability between other published δ^{98}Mo values for ocean water are probably due to different standards used in different laboratories, rather than a reflection of true ocean water heterogeneity (cf. Greber et al. 2012, Nakagawa et al., 2012). In the standardisation used here, the Mo isotope ocean water value is +2.34 ‰ (see Methods). Mo isotopes have been shown to fractionate negatively from modern ocean water ($\alpha Mo_{sorb} - MoO_4^{-2}$ = 0.997) down to δ^{98}Mo values of -0.1 to -0.8‰ through surface adsorption to Mn-oxides (e.g., Barling and Anbar, 2004). Fractionation on the surface of hematite, goethite or ferrihydrite (Goldberg et al., 2009) is somewhat smaller ($\alpha Mo_{sorb} - MoO_4^{-2}$ = 0.998, 0.9985, and 0.999 respectively). By comparison, δ^{98}Mo signatures from modern sediments deposited under high sulfide concentrations show much less fractionation from modern seawater (Neubert et al., 2008), essentially preserving the seawater Mo isotopic composition.

The δ^{98}Mo values from samples low in the stratigraphic section (-0.22 to +0.06‰) show a range that would be expected from hematite-based Mo scavenging from ocean water with a modern Mo isotopic composition. The δ^{98}Mo signatures documented at the top of the iron formation (+0.51 to +0.71‰), however, fall firmly in the range for recent suboxic sediments that trend towards anoxic conditions (Poulson et al., 2006), and are significantly heavier than is expected in hematite-rich rocks.

According to scientific consensus, iron formation was formed by Fe^{2+} transformation to Fe^{3+} at a mixing zone with oxidizing seawater, precipitating as $Fe(OH)_3$-particles. The phase that most closely resembles this among the Fe-precipitates investigated by Goldberg et al. (2009) might therefore be goethite. However, the solid Fe-phase observed in the Rapitan IF is exclusively hematite. The basis for most models of oxide-facies IF is that the $Fe(OH)_3$-particles dehydrated to hematite prior to compaction. Therefore, oxide facies BIF should preserve pre-compaction particles of hematite (Krapež et al., 2003). Furthermore, the preservation of primary sedimentary textures in the hematite in samples analysed here suggests that the precursor mineral converted to hematite very early (Fig. 2A, B, C). Even if does not form in the water column, but is the product of the transformation of an earlier metastable phase, hematite re-equilibrates with

ocean water as long as it stays in contact with bottom water. Therefore, we consider hematite to be the relevant stable Fe-phase in further discussion. According to Goldberg et al. (2009), the adsorption of Mo on hematite results in a negative fractionation of 1.8‰ to 2.0‰, unless extreme removal is assumed.

4. Discussion

4.1 Metal enrichments, Re and δ^{98}Mo

A proper understanding of the implications of the documented Re and δ^{98}Mo compositions of the Rapitan iron formation requires direct comparison to other, simpler redox proxies, such as the authigenic elemental enrichments of the redox-sensitive Mo and U, expressed as unitless enrichment factors (Mo_{EF} and U_{EF}, respectively). In this study, enrichment factors were calculated by double-normalising Mo and U to the Al concentration and the upper continental crust composite MuQ (an alluvial sediment average, Kamber et al., 2005), using the formula $EF= ([X]_{sample}/Al_{sample})/([X]_{MuQ}/Al_{MuQ}$, X= either Mo or U concentrations (cf., Algeo and Tribovillard, 2009 and ref. within). Comparison to these elements is particularly useful, in that their behaviour in marine systems is well understood, and their redox sensitivities bracket those of Re, and also because enrichments of Mo and U have been a crucial line of evidence in the development of recent depositional models for Neoproterozoic IF (e.g., Baldwin et al., 2012).

The stratigraphic distribution of Re concentrations is similar to U enrichment factors throughout the thickness of the iron formation (Fig. 3). This covariation is because both elements are fixed under suboxic to non-sulfidic anoxic conditions, although Re requires slightly more reducing conditions for its fixation than does U. At the base and middle of the section, both elements show low to moderate enrichments (U) or concentrations (Re), but both values increase towards the top of the IF. Uranium, although only modestly enriched overall, shows its strongest enrichment at the bottom and in the middle of the section. Zones of increased U enrichment probably record open marine conditions at a redox level in the vicinity of Fe oxidation, because U and Fe oxidise at approximately similar O_2 levels, although below this threshold U fixation increases, whereas Fe solubility increases. Thus, horizons with the lowest U enrichment may

record the zones of greatest iron oxidation and fixation. The general increase in U enrichment and substantial increase in Re concentration at the top of the iron formation indicate that marine conditions became more anoxic near the end of iron formation deposition.

Rhenium also roughly mirrors the distribution of the Mo_{EF} throughout much of the iron formation. The main difference is the elevated Mo enrichment at the base of the section, which has been interpreted to reflect brief, mildly sulfidic conditions at middle water depths immediately following glacial ice withdrawal (Baldwin et al., 2012), without driving significant Re fixation. Thus, it can also be assumed that adsorption of dissolved Mo and Mo-bearing phases onto Fe colloids may have been a factor. This is reflected by the weak correlation between Fe_2O_3 and Mo in samples with moderately high concentrations of both (Baldwin et al., 2012), resulting in elevated Mo enrichment at the bottom of the section without commensurate Re enrichment. The pronounced increase in both the Re/Mo ratio and δ^{98}Mo, paired with very low Mo enrichment may at first seem counterintuitive. The most obvious explanation is that this arrangement could reflect a decrease in the oxidation state of the water column towards increased ferruginous conditions. Decreased production of Fe oxy-hydroxides would accompany an increase in ferruginous conditions and would limit both the Mo fixation rate (explaining the low Mo_{EF}), as well as the influence of hematite on the Mo isotopic budget, thereby allowing an increase in δ^{98}Mo. This change would have been short-lived and fairly mild. Although the Re/Mo ratios show a strong increase, this is less driven by an increase in Re fixation, and much more strongly caused by the decrease in Mo fixation rates. Thus, this brief increase in Re/Mo and δ^{98}Mo can be explained as a decrease in the Fe oxy-hydroxide production rate due to a brief, slight decrease in oxygen availability in the water column. At the top of the iron formation, however, both Re concentrations and Mo_{EF} show a marked increase, which is coincident with elevated U_{EF} values and Re/Mo ratios that are comparable to those of modern seawater. The increased Mo enrichment at this stratigraphic level, paired with the seawater Re/Mo values, shows that marine conditions during deposition of the uppermost iron formation beds were rapidly transitioning from an oxic to suboxic/anoxic regime towards mildly sulfidic conditions.

If it is accepted that adsorption to hematite was the dominant fractionation process of Mo isotopes at the base and throughout most of the middle of the iron formation, an ocean water Mo

isotope composition of around +1.8‰ can be inferred from the light δ^{98}Mo signatures in the jasper. The three stratigraphically highest samples, however, show higher δ^{98}Mo values, from +0.51 to +0.71‰. Other proxies from these samples (Mo_{EF} and Re/Mo) indicate mildly sulfidic conditions. This apparent mutual inconsistency between the δ^{98}Mo and trace element enrichments could be resolved if deposition of significant volumes of hematite or other iron oxy-hydroxides continued at this stratigraphic level. In summary, the data are best explained if hematite deposition and (weakly) sulfidic water conditions coexisted.

Four hypotheses may help to explain the increased δ^{98}Mo values that accompany increasing anoxia at the top of the section:

1) Seawater δ^{98}Mo increased by ~0.7‰;

2) Diagenetic effects were imposed by the overlying diamictite;

3) The δ^{98}Mo of local water increased by 0.7‰ due to increased Mo sequestration (basin effect);

4) Alpha, (the fractionation factor) changed.

Considering hypothesis 1 first, we note that a general increase of the seawater δ^{98}Mo cannot be definitively tested using the present data set. However, a sudden increase by about 0.7‰, coincident with a local change in redox conditions, appears to be an *ad hoc* assumption with relative low probability.

With regard to hypothesis 2, it is important to recall that the trend in all geochemical proxies towards an anoxic water column occurs exclusively in the uppermost metre of the iron formation. The iron formation is immediately overlain by non-hematitic glacioclastic sediment (Fig. 1B, C), which therefore do not have the strong negative Mo isotope fractionation to Fe-phases. The heavier δ^{98}Mo composition (and the rest of the chemical proxies) from the top of the section could be diagenetically mixed with the pore water of the glacioclastic sediment, which was shown to be possible in Goldberg et al. (2012). The possibility of diagenesis strongly influencing the δ^{98}Mo composition is deemed less probable, based on the fact that the top of the

iron formation was mostly lithified before the diamictite was deposited, as shown by the presence of angular, reworked jasper clasts low in the diamictite.

Addressing hypothesis 3 (basin effect), the key criterion is that a δ^{98}Mo increase of the local water by 0.7‰ would require that the basin was becoming restricted and that significantly more Mo was being sequestered. For example, Nägler et al. (2011) showed that in the Black Sea the anoxic water mass has a δ^{98}Mo composition of about 0.4 to 0.6‰ above mean open ocean water. However, for the IF studied here, REE+Y patterns (reported in Baldwin et al. 2012) do not change stratigraphically, and lack evidence for increasing water restriction overall. Hydrogenous sedimentary rocks from epi-continental basins have REE+Y patterns that are different from those of the open ocean (e.g., Kamber et al., 2004). Furthermore, covariance plots between δ^{98}Mo and several trace element proxies (Mo, Mo_{EF}, Re, and Re/Mo) clearly demonstrate that their enrichment is independent of the Mo isotopic composition: samples with elevated δ^{98}Mo (δ^{98}Mo > 0.20‰) form a distinct sub-parallel to non-parallel trend with respect to each of these proxies from samples with lower δ^{98}Mo values (Fig. 4A-D). Not only does this support the independence of the trace element proxies from the processes that drove Mo isotopic fractionation, it also dissociates the δ^{98}Mo values from both the absolute Mo concentrations and relative Mo enrichment (Fig 4A, B). This strongly indicates that under all redox conditions, the δ^{98}Mo signature of the sediment was controlled by processes that were distinct from those that controlled the elemental redox proxies. These observations render the basin effect an improbable explanation for the documented Mo isotope stratigraphy.

Finally, concerning hypothesis 4, it is important to recall that in general terms the Mo isotope fractionation factor can vary based on the redox condition of the water (e.g., Nägler et al., 2011; Neubert et al., 2008; Poulson et al., 2006). However, most studies attribute such fractionation to the formation of authigenic Fe-sulfides in the water column or in pore waters under anoxic water columns. In the studied jasper, all samples are consistently composed of quartz and hematite, and so a change of the fractionation factor that is tied to changes in the mineral precipitate species can be excluded. It has to be considered, though, that Mo isotope fractionation factors for adsorption on hematite under reducing conditions are not known. Apparently, as the seawater at the time of the uppermost part of the Rapitan IF was turning

anoxic, its δ^{98}Mo signature adjusted to the smaller Mo isotope fractionation factor that prevailed under such conditions.

In summary, the first three hypotheses are all counter-indicated to various extents by other evidence, leaving the fractionation factor model as the only possible explanation. Given the non-actualistic formation of these sedimentary rocks, a firm conclusion on the mechanistic processes resulting in a change of the fractionation factor (hypothesis 4) cannot be drawn. However, this hypothesis is compatible with all observations made: it explains the documented shift in δ^{98}Mo based on observed changes in the water column, is not in conflict with the elemental redox proxies that record a shift towards anoxia, and results in Mo isotopic signatures that are significantly heavier than is typical for hematite adsorption, but which are also lighter than the ambient Mo isotopic composition of seawater.

4.2 Implications for Neoproterozoic iron formation

The trace element and Mo isotopic data show that throughout the majority of iron formation deposition, marine redox conditions in the basin were predominantly driven by a combination of oxic and ferruginous conditions, as reflected by the large volume of hematite deposited in the iron formation, together with the low Mo enrichments, Re concentrations, and Re/Mo ratios. At the top of the iron formation, however, all available proxies indicate that the basin conditions were becoming anoxic to slightly sulfidic. The marked increase in the fixation rates of U, Mo, and Re shows that the redox state of the water column dropped well below the oxygen levels required for the oxidation of Fe^{2+} to Fe^{3+}. This pattern is perhaps best illustrated by the elevated Re/Mo ratios, which are comparable to those of modern seawater. Furthermore, the shift towards markedly positive δ^{98}Mo values shows a decreased fractionation from presumed ambient seawater conditions, with a maximum δ^{98}Mo of +0.71‰. This value is only slightly lower than previous estimates for the Mo isotopic composition for Mesoproterozoic (0.8‰; Arnold et al., 2004) and early Neoproterozoic (1.0 ± 0.1‰; Dahl et al., 2011) seawater. Sulfidic conditions were gradually driving more complete Mo fixation, with an evolving fractionation factor, thus recording different δ^{98}Mo than would be expected based on the continued deposition

of large volumes of iron oxy-hydroxides. The most important aspect of this shift is the fact that the heavy Mo isotopes and seawater Re/Mo ratios are preserved in samples at the very top of the iron formation, which is immediately overlain by *non-hematitic* glacioclastic sediment (Fig 1B, C). The abrupt termination of hematite deposition suggests either that the Fe^{2+} inventory in the Rapitan basin had been drawn down such that there was insufficient supply to continue depositing sedimentary iron (as iron formation or hematitic clastic sediment), or that the recorded shift towards increasingly anoxic conditions abruptly terminated the oxidation of dissolved Fe^{2+} to Fe^{3+}, thereby keeping the iron in solution. This second explanation is more plausible due to its consistency with the other redox proxy data.

The observed shift away from oxic and ferruginous conditions, as recorded by the elemental proxies (Mo enrichment and Re/Mo) was not responsible for the termination of iron formation deposition across the entire basin. In Yukon, west of the study site, the uppermost strata of the iron formation consists of granular iron formation (GIF) (Baldwin and Turner, 2012; Klein and Beukes, 1993), which is in turn overlain by hematitic glacioclastic rocks. This relationship indicates that in some areas, particularly where the preserved iron formation is thickest, loss of accommodation space was probably the driving force behind the cessation of pure iron formation deposition. As accommodation space diminished, the clastic sedimentation rate to the deep basin increased, which would have volumetrically overwhelmed the background iron and silica precipitation, forming hematitic clastic rocks in lieu of iron formation. Thus, deposition of thick iron formation represents a condition of a perfect balance of ferruginous to oxic basinal redox conditions, a limited clastic sediment supply, and ample accommodation space. Elimination of any of these features, even at the local scale, apparently caused the fairly abrupt cessation of iron formation deposition.

4.3 Mo isotopic composition of the Neoproterozoic ocean

It has been suggested that Proterozoic seawater had a significantly lighter Mo isotopic composition than the modern ocean (e.g., Dahl et al., 2011). This proposal was based on several studies of Meso- and Neoproterozoic black shales that have been shown to be sulfidic using other proxies (e.g., iron speciation). These studies have shown that sulfidic shales from this time have δ^{98}Mo values more than 1.0‰ lighter (Arnold et al., 2004; Dahl et al., 2011), than the

436 modern seawater value of +2.34‰ (Siebert et al., 2003; Greber et al., 2012), suggesting that
437 seawater δ^{98}Mo remained stable at approximately 1.0‰ throughout the Proterozoic. The
438 explanation for this apparent difference in seawater isotope composition is that more widespread
439 sulfidic conditions in the Proterozoic would have resulted in an overall depletion of ^{98}Mo in
440 seawater, leaving a lighter ambient δ^{98}Mo composition in normal marine seawater, which in turn
441 was recorded in sulfidic black shales. A few of the samples analysed here have values similar to
442 those of many samples reported in Dahl et al. (2011), which were interpreted to record sulfidic
443 conditions based on iron speciation data, and were thought to record ambient seawater δ^{98}Mo
444 values. Thus, these authors proposed that the δ^{98}Mo composition of Neoproterozoic seawater
445 was approximately 1.0±0.1‰. This claim is problematic for two reasons. First, Dahl et al. (2011)
446 used an unusually low threshold in their iron speciation data (Fe_P/Fe_{HR} = 0.5) to distinguish
447 sulfidic from suboxic to anoxic shales, on the grounds that the majority of the reactive iron is
448 pyrite. Conventionally, a higher threshold of 0.7-0.8 is applied, to help eliminate the influence of
449 diagenetic sulfidisation (Poulton and Canfield, 2011). Very few of the samples analysed by Dahl
450 et al. (2011) meet the conventional threshold for this ratio, making the bulk of the dataset
451 indicative of ferruginous rather than sulfidic conditions. This allows for the possibility that very
452 little of their data records the true seawater δ^{98}Mo signature. Furthermore, Dahl et al. (2011) do
453 not address why they preferred to assume an ocean water composition of 1.0‰, even though
454 their own detritus-corrected data for true sulfidic samples (Fe_P/Fe_{HR} >0.7) is 1.25±0.40. The
455 second problem is that samples analysed by Dahl et al. (2011) with Fe_P/Fe_{HR} significantly below
456 the criterion for sulfidic conditions (down to 0.0), also show the same δ^{98}Mo data as those few
457 samples that supposedly represent ocean water. As shown by earlier publications, Mo isotope
458 fractionation inevitably occurs under anoxic, non-sulfidic conditions (e.g., Poulson et al. 2006)
459 or conditions with H_2S_{aq} below the threshold value of 11 µM H_2S_{aq} (Neubert et al., 2008). For
460 example, in the Black Sea, at 400 m water depth, including a 250 m-thick sulfidic layer,
461 sediment still records a δ^{98}Mo of 0.7‰ below seawater values, due to insufficient H_2S
462 concentration. The most plausible explanation would be that the whole sequence adjusted its
463 δ^{98}Mo values during diagenesis under anoxic waters (indicated by the semi-constant Fe_{HR}/Fe_T),
464 which would imply a coeval seawater value of 0.7‰ above the sedimentary average (Poulson et

al. 2006). We here maintain that this interpretation of Dahl et al. (2011) is not unique and the data are not incompatible with coeval ocean water δ^{98}Mo of ~1.8‰.

Taken at face value, the δ^{98}Mo data from the most anoxic samples published here fall into a similar range as the samples used by Dahl et al. (2011) to establish their proposed Neoproterozoic seawater composition. Although some of these samples record probable sulfidic conditions, as indicated by the Mo_{EF} and Re/Mo data, they are also hematite-rich rocks (i.e., iron formation and jasper). This geological constraint, together with the redox proxy data and the presence of primary to very early diagenetic hematite, has important implications. Namely, across the entire basin, iron formation deposition was not stratigraphically coherent. Instead, a subtle interplay between basin subsidence, the relative proportion of clastic and hydrogenous sediment supply, elemental inventories (i.e., Fe and S), and ice cover resulted in variable deposition of Fe-rich rocks. Unusual basinal redox situations existed at a local scale and may be represented by IF horizons, which are appropriate for geochemical investigations owing to the lack of interfering clastic sediment. Such unusual redox situations had a profound effect on the typical processes controlling Mo isotopic behaviour. Qualitatively at least, it is evident that Mo isotopes in rocks containing hydrogenous hematite (or other Fe-oxides) show lighter isotopic compositions than coeval seawater, as is clearly recorded throughout most of the lower part of the Rapitan iron formation. Jasper samples with relatively heavy Mo isotopic signatures, therefore, must similarly be negatively fractionated from ambient seawater, regardless of the basinal redox conditions. It is impossible to quantify the ocean water Mo isotope signature from these anoxic samples, because the corresponding fractionation factor cannot be independently defined.

Heavy δ^{98}Mo signatures in the Rapitan IF record the interplay between two opposing fractionation mechanisms. Although the ambient sulfidic conditions in the water column apparently limited the fractionation away from the seawater composition, the continued rain of iron oxide/oxy-hydroxide flocculates through the sulfidic part of the water column from overlying oxic waters (Baldwin et al., 2012) still preferentially fixed light Mo, even under conditions favourable to complete, unfractionated fixation. The net result of these processes would be a sedimentary δ^{98}Mo composition that is significantly lighter than that of seawater, but

494 also much higher than would be recorded under oxic to ferruginous conditions during normal
495 hematite deposition, as is seen in the samples from the top of the iron formation, which have
496 δ^{98}Mo of +0.7‰. Thus, although the highest δ^{98}Mo values reported here are lower than the
497 previously proposed δ^{98}Mo composition of the Neoproterozoic ocean (1.0±0.1‰), they clearly
498 indicate that the isotopic composition must have been still higher than that, and much closer to
499 that of the modern ocean. Although the Rapitan iron formation was deposited in a partly
500 restricted rift basin, REE+Y data show that there was significant connectivity between the
501 Rapitan basin and the open ocean (Baldwin et al., 2012). It is reasonable to assume that a basin
502 with moderate to high connectivity with the open ocean would have had the same isotopic
503 composition as the global ocean. Therefore, as a working hypothesis, it can be inferred that
504 global mid-Neoproterozoic seawater had a δ^{98}Mo composition of approximately 1.8‰, which is
505 not much lower than that of the modern ocean. If true, this analogy to modern oceans implies a
506 homogeneous ocean water composition. On the surface, this assumption is challenged by the
507 possibility that, during the Neoproterozoic, the residence time of Mo was significantly shorter
508 owing to a limited Mo ocean inventory. However, even if the Neoproterozoic Mo inventory was
509 only 10% of that of the modern ocean (as suggested by Scott et al., 2009), the residence time of
510 Mo would still be at least 44 k.y., based on a residence time of Mo in modern seawater of 440
511 k.y. This latter value, put forward by Miller et al, (2011), is the lowest proposed in recent
512 literature. To allow for significant heterogeneity of the ocean water in terms of Mo isotopic
513 composition, the ocean mixing time would have to have been in the range of the Mo residence
514 time. Of course the true mixing time of the Neoproterozoic oceans is not known. A mixing time
515 of 44 k.y., however, would be about 30 times longer than that of modern oceans. This is hardly
516 realistic if there was any connectivity among the Neoproterozoic oceans at all. Thus, even if the
517 Neoproterozoic Mo inventory was only 10% of the modern ocean, the resulting shorter residence
518 time does not challenge the assumption of a nearly uniform ocean water Mo isotopic
519 composition.

520 A near-modern marine Mo isotopic composition in the middle Neoproterozoic indicates
521 that the deep ocean was already ventilated at that time. If the Neoproterozoic weathering regime
522 of Mo was comparable to that of today, the principal control on the δ^{98}Mo composition of
523 seawater would have been the generation of Mn and Fe oxy-hydroxides, and the subsequent

adsorption of isotopically light Mo to these particles. This stands in sharp contrast with arguments for a lighter seawater δ^{98}Mo composition in the Neoproterozoic, which require moderately extensive, nearshore sulfidic water masses to limit the amount of heavy Mo in seawater (Dahl et al., 2011). Thus, the data presented here suggest that sulfidic conditions in the open ocean during the middle Neoproterozoic could have been only slightly more pervasive than today. Taken together with the well-established absence of the positive Eu anomaly in Neoproterozoic iron formations (e.g., Baldwin et al., 2012; Klein and Beukes, 1993; Klein and Ladeira, 2004; Lottermoser and Ashley, 2000), it appears that in the middle Neoproterozoic the open ocean was well oxygenated, and that ferruginous and sulfidic conditions were limited to restricted and semi-restricted basin environments. The strong evidence for pervasive anoxia in the Ediacaran ocean (e.g., Canfield et al., 2008) suggests a post-"snowball Earth" return to more widespread reduced marine conditions.

5. Conclusions

Evidence from Re concentrations, Re/Mo ratios, and Mo isotope ratios shows that the prevailing basin redox conditions during deposition of the Rapitan iron formation were ferruginous trending towards oxic. Rhenium concentrations and Re/Mo ratios are consistently low throughout most of the thickness of the iron formation. Near the top of the section, however, both values increase by several orders of magnitude, recording a shift away from oxic to ferruginous conditions and towards anoxic to sulfidic conditions. Similarly, most of the iron formation has negative to mildly positive δ^{98}Mo compositions, most likely because adsorption to hematite was the primary cause of Mo isotopic fractionation. At the top of the iron formation, the δ^{98}Mo composition increases to +0.7‰, which, when considered together with other redox proxies (Mo enrichment, Re concentrations, and Mo/Re), records sulfidic conditions. The observed shift to sulfidic conditions, paired with the presence of non-hematitic glacioclastic sediments above the iron formation, indicates that these conditions locally terminated the deposition of iron formation. Correcting the δ^{98}Mo value for the isotope fractionation that occurs during adsorption to iron oxy-hydroxides, the Mo isotope composition of the Neoproterozoic

552 ocean was around 1.8‰. A middle Neoproterozoic ocean with such δ^{98}Mo values indicates that
553 the open ocean may have been well oxygenated at 700 Ma.

554

555 Acknowledgements

556 This paper is Northwest Territories Geoscience Office contribution number 0065. Field
557 work was supported by the Northwest Territories Geoscience Office (NTGO) and Yukon
558 Geological Survey (YGS). Substantial funding was also provided by National Science and
559 Engineering Research Council of Canada (NSERC) Discovery Grants to ECT and BSK, as well
560 as a Society of Economic Geologists (SEG) student research grant to GJB. This paper benefitted
561 greatly from the comments of editor R.R. Parrish and an anonymous reviewer. A. Gladu and J.A.
562 Petrus are thanked for their assistance in the lab at Laurentian University. The ^{185}Re metal spike
563 was supplied by O.M. Burnham of the Ontario Geoscience Laboratories (GeoLabs).

564

565 Figure Captions

566 Figure 1: Map showing the distribution of Proterozoic sedimentary rocks in north-western
567 Canada. The <716 Ma glaciogenic Rapitan Group is in red (from Baldwin et al., 2012), with an
568 arrow indicating the location of the study area (A). Sharp upper contact between the Rapitan iron
569 formation and the overlying non-hematitic glacioclastic rocks of the overlying Shezal Formation
570 (B, C). The contact is partly obscured in each photo due to the recessive weathering character of
571 the glacioclastics, but is indicated by an arrow in (B). Purple area on the cliff face in each photo
572 is an area of reworked iron formation contained as a raft in the overlying glacioclastics; this unit
573 is laterally discontinuous, as seen in each photograph.

574 Figure 2: Photographs (A, B) and a photomicrograph (C) showing the preservation of primary
575 sedimentary fabrics in hematite, suggesting a depositional or early diagenetic origin. Deformed
576 bedding from a dropstone is preserved (A). Fine laminations in hematite visible on the outcrop
577 scale (B) and sub-millimetre scale (C) around chert and carbonate nodules. Late conversion to
578 hematite from precursor minerals would overprint some of these finer textures.

Figure 3: Simplified stratigraphic column of section CR1 (after Baldwin et al., 2012) with stratigraphic distributions of Mo_{EF}, U_{EF}, Re (ppt), Re/Mo, and $\delta^{98}Mo$ (‰). Mo, U, and Al concentration data (used to calculate enrichment factors and Re/Mo) are from Baldwin et al. (2012). With the exception of the moderate to strong Mo enrichment at the base of the section, Mo enrichment and Re concentration covary, both showing a pronounced increase at the top of the section. With the exception of the uppermost samples, the Re/Mo ratio is well below the modern seawater ratio of $8.0x10^{-4}$ (dashed line), but the uppermost samples are close to this value, recording sulfidic conditions. $\delta^{98}Mo$ (with 2σ error bars) is scattered between -0.2 and 0.1‰, recording sulfidic conditions paired with adsorption to hematite, except for a few higher values, most notably at the top of the section.

Figure 4: Covariance plots of $\delta^{98}Mo$ vs. Mo concentration (A), Mo enrichment (B), Re concentration (C), and Re/Mo (D). Samples with positive $\delta^{98}Mo$ form distinct trends relative to all other proxies from samples with near-zero to negative $\delta^{98}Mo$ values.

References

Algeo, T.J. and Tribovillard, N., 2009. Environmental analysis of paleoceanographic systems based on molybdenum-uranium covariation. Chemical Geology, 268: 211-225.

Arnold, G.L., Anbar, A.D., Barling, J. and Lyons, T.W., 2004. Molybdenum isotope evidence for widespread anoxia in mid-Proterozoic oceans. Science, 304: 87-90.

Baldwin, G.J., Thurston, P.C. and Kamber, B.S., 2011. High-precision rare earth element, nickel, and chromium chemistry of chert microbands pre-screened with in-situ analysis. Chemical Geology, 285: 133-143.

Baldwin, G.J. and Turner, E.C., 2012. Lithofacies and lithostratigraphic correlation potential of the Rapitan iron formation, Snake River area (NTS 106F), Yukon. In: K.E. Macfarlane and P.J. Sack (Editors), Yukon Exploration and Geology 2011. Yukon Geological Survey, pp. 1-15.

Baldwin, G.J., Turner, E.C. and Kamber, B.S., 2012. A new depositional model for glaciogenic Neoproterozoic iron formation: insights from the chemostratigraphy and basin configuration of the Rapitan iron formation. Canadian Journal of Earth Sciences, 49: 455-476.

Barling, J. and Anbar, A.D., 2004. Molybdenum isotope fractionation during adsorption by manganese oxides. Earth and Planetary Science Letters, 217: 315-329.

Barling, J., Arnold, G.L. and Anbar, A.D., 2001. Natural mass-dependent variations in the isotopic composition of molybdenum. Earth and Planetary Science Letters, 193: 447-457.

Bekker, A. et al., 2010. Iron formation: The sedimentary product of a complex interplay among mantle, tectonic, oceanic, and biospheric processes. Economic Geology, 105: 467-508.
Bekker, A. et al., 2004. Dating the rise of atmospheric oxygen. Nature, 427: 117-120.
Canfield, D.E., 1998. A new model for Proterozoic ocean chemistry. Nature, 396: 450-453.
Canfield, D.E. et al., 2008. Ferruginous conditions dominated later Neoproterozoic deep-water chemistry. Science, 321: 949-952.
Canfield, D.E., Poulton, S.W. and Narbonne, G.M., 2007. Late-Neoproterozoic deep-ocean oxygenation and the rise of animal life. Science, 315: 92-95.
Crusius, J., Calvert, S., Pedersen, T. and Sage, D., 1996. Rhenium and molybdenum enrichments in sediments as indicators of oxic, suboxic, and sulfidic conditions of deposition. Earth and Planetary Science Letters, 145: 65-78.
Dahl, T.W. et al., 2011. Molybdenum evidence for expansive sulfidic water masses in ~750 Ma oceans. Earth and Planetary Science Letters, 311: 264-274.
Fischer-Gödde, M., Becker, H. and Wombacher, F., 2011. Rhodium, gold and other highly siderophile elements in orogenic peridotites and peridotite xenoliths. Chemical Geology, 280: 365-383.
Goldberg, T., Archer, C., Vance, D. and Poulton, S.W., 2009. Mo isotope fractionation during adsorption to Fe (oxyhydr)oxides. Geochimica et Cosmochimica Acta, 73: 6502-6516.
Goldberg, T. et al., 2012. Controls on Mo isotope fractionations in a Mn-rich anoxic marine sediment, Gullmar Fjord, Sweden. Chemical Geology, 296-297: 73-82.
Greber, N.D., Hofmann, B.A., Voegelin, A.R., Villa, I.M. and Nägler, T.F., 2011. Mo isotope composition in Mo-rich high- and low-T hydrothermal systems from the Swiss Alps. Geochimica et Cosmochimica Acta, 75(21): 6600-6609.
Greber, N.D., Siebert, C., Nägler, T.F. and Pettke, T., 2012. $\delta^{98/95}$ Mo values and molybdenum concentration data for NIST SRM 610, 612, and 3134: towards a common protocol for reporting Mo data. Geostandards and Geoanalytical Research, 36(3): 291-300.
Johnston, D.T. et al., 2010. An emerging picture of Neoproterozoic ocean chemistry: Insights from the Chuar Group, Grand Canyon, USA. Earth and Planetary Science Letters, 290: 64-73.
Kamber, B.S., Bolhar, R. and Webb, G.E., 2004. Geochemistry of late Archean stromatolites from Zimbabwe: evidence for microbial life in restricted epicontinental seas. Precambrian Research, 132(4): 379-399.
Kamber, B.S., Greig, A. and Collerson, K.D., 2005. A new estimate for the composition of weathered young upper continental crust from alluvial sediments, Queensland, Australia. Geochimica et Cosmochimica Acta, 69(4): 1041-1058.
Kirschvink, J.L., 1992. Late Proterozoic low-latitude global glaciation: the Snowball Earth. In: J.W. Schopf and C. Klein (Editors), The Proterozoic biosphere: A multidisciplinary study. Cambridge University Press, Cambridge, pp. 51-52.
Klein, C. and Beukes, N.J., 1993. Sedimentology and geochemistry of the glaciogenic late Proterozoic Rapitan iron-formation in Canada. Economic Geology, 88: 542-565.
Klein, C. and Ladeira, E.A., 2004. Geochemistry and mineralogy of Neoproterozoic banded iron-formations and some selected, silicieous manganese formations form the Urucum District, Mato Grosso Do Sul, Brazil. Economic Geology, 99: 1233-1244.
Krapež, B., Barley, M.E. and Pickard, A.L., 2003. Hydrothermal and resedimented origins of the precursor sediments to banded iron formation: sedimentological evidence from the Early

Palaeoproterozoic Brockman Supersequence of Western Australia. Sedimentology, 50(5): 979-1011.
Li, C. et al., 2010. A stratified redox model for the Ediacaran ocean. Science, 328: 80-83.
Lottermoser, B.G. and Ashley, P.M., 2000. Geochemistry, petrology and origin of Neoproterozoic ironstones in the eastern part of the Adelaide Geosyncline, South Australia. Precambrian Research, 101: 49-67.
Macdonald, F.A. et al., 2010a. Calibrating the Cryogenian. Science, 327: 1241-1243.
Macdonald, F.A., Strauss, J.V., Rose, C.V., Dudás, F.Ö. and Schrag, D.P., 2010b. Stratigraphy of the Port Nolloth Group of Namibia and South Africa and implications for the age of Neoproterozoic iron formations. American Journal of Science, 310: 862-888.
Meisel, T., Dale, C.W., Pearson, D.G. and Sergeev, D.S., 2009. Complete sample digestions for accurate isotope measurements? The Re-Os isotope system under scrutiny. Geochimica et Cosmochimica Acta, 73(13): A867.
Meisel, T. and Moser, J., 2004. Platinum-group element and rhenium concentrations in low abundance reference materials. Geostandards and Geoanalytical Research, 28(2): 233-250.
Miller, C.A., Peucker-Ehrenbrink, B., Walker, B.D. and Marcantonio, F., 2011. Re-assessing the surface cycling of molybdenum and rhenium. Geochimica et Cosmochimica Acta, 75(22): 7146-7179.
Morford, J.L. and Emerson, S., 1999. The geochemistry of redox sensitive trace metals in sediments. Geochimica et Cosmochimica Acta, 63(11/12): 1735-1750.
Morford, J.L., Emerson, S.R., Breckel, E.J. and Kim, S.H., 2005. Diagenesis of oxyanions (V, U, Re, and Mo) in pore waters and sediments from a continental margin. Geochimica et Cosmochimica Acta, 69(21): 5021-5032.
Nägler, T.F., Neubert, N., Böttcher, M.E., Dellwig, O. and Schnetger, B., 2011. Molybdenum isotope fractionation in pelagic euxinia: Evidence from the modern Black and Baltic Seas. Chemical Geology, 289: 1-11.
Nakagawa, Y. et al., 2012. The molybdenum isotopic composition of the modern ocean. Geochemical Journal, 46(2): 131-141.
Nameroff, T.J., Balistrieri, L.S. and Murray, J.W., 2002. Suboxic trace metal geochemistry in the eastern tropical North Pacific. Geochimica et Cosmochimica Acta, 66(7): 1139-1158.
Neubert, N., Nägler, T.F. and Böttcher, M.E., 2008. Sulfidity controls molybdenum isotope fractionation into euxinic sediments: Evidence from the modern Black Sea. Geology, 36(10): 775-778.
Och, L.M. and Sheilds-Zhou, G.A., 2012. The Neoproterozoic oxygenation event: Environmental perturbations and biogeochemical cycling. Earth-Science Reviews, 110: 26-57.
Pattan, J.N. and Pearce, N.J.G., 2009. Bottom water oxygenation history in southeastern Arabian Sea during the past 140 ka: Results from redox-sensitive elements. Palaeogeography, Palaeoclimatology, Palaeoecology, 280: 396-405.
Planavsky, N.J. et al., 2011. Widespread iron-rich conditions in the mid-Proterozoic ocean. Nature, 477: 448-451.
Poulson, R.L., Siebert, C., McManus, J. and Berelson, W.M., 2006. Authigenic molybdenum isotope signatures in marine sediments. Geology, 34(8): 617-620.

Poulton, S.W. and Canfield, D.E., 2011. Ferruginous conditions: a dominant feature of the ocean through Earth's history. Elements, 7: 107-112.

Poulton, S.W., Fralick, P.W. and Canfield, D.E., 2004. The transition to a sulphidic ocean ~1.84 billion years ago. Nature, 431: 173-177.

Poulton, S.W., Fralick, P.W. and Canfield, D.E., 2010. Spatial variability in oceanic redox structure 1.8 billion years ago. Nature Geoscience, 3: 486-490.

Scott, C. et al., 2008. Tracing the stepwise oxygenation of the Proterozoic ocean. Nature, 452: 456-459.

Shen, Y., Canfield, D.E. and Knoll, A.H., 2002. Middle Proterozoic ocean chemistry: evidence from the McArthur basin, Northern Australia. American Journal of Science, 302: 81-109.

Siebert, C., Nägler, T.F. and Kramers, J.D., 2001. Determination of molybdenum isotope fractionation by double-spike multicollector inductively coupled plasma mass spcetometry. Geochemistry, Geophysics, Geosystems, 2: doi:10.1029/2000GC000124.

Siebert, C., Nägler, T.F., von Blanckenburg, F. and Kramers, J.D., 2003. Molybdenum isotope records as a potential new proxy for paleoceanography. Earth and Planetary Science Letters, 211: 159-171.

Slack, J.F., Grenne, T., Bekker, A., Rouxel, O.J. and Lindberg, P.A., 2007. Suboxic deep seawater in the late Paleoproterozoic: Evidence from hematitic chert and iron formation related to seafloor-hydrothermal sulfide deposits, central Arizona, USA. Earth and Planetary Science Letters, 255: 243-256.

Wille, M. et al., 2007. Evidence for a gradual rise of oxygen between 2.6 and 2.5 Ga from Mo isotopes and Re-PGE signatures in shales. Geochimica et Cosmochimica Acta, 71: 2417-2435.

Figure

Click here to download high resolution image

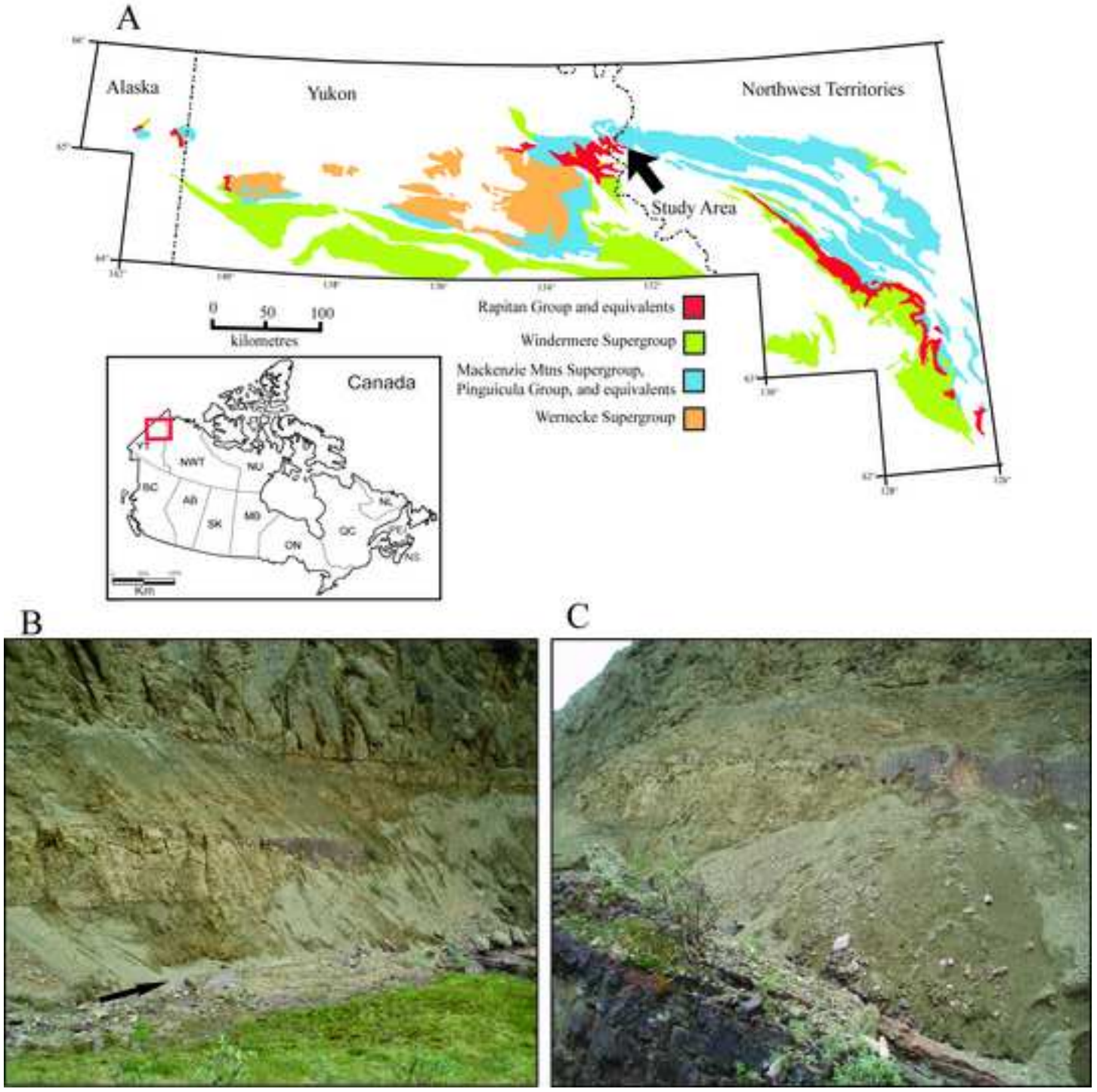

Figure 2

Click here to download high resolution image

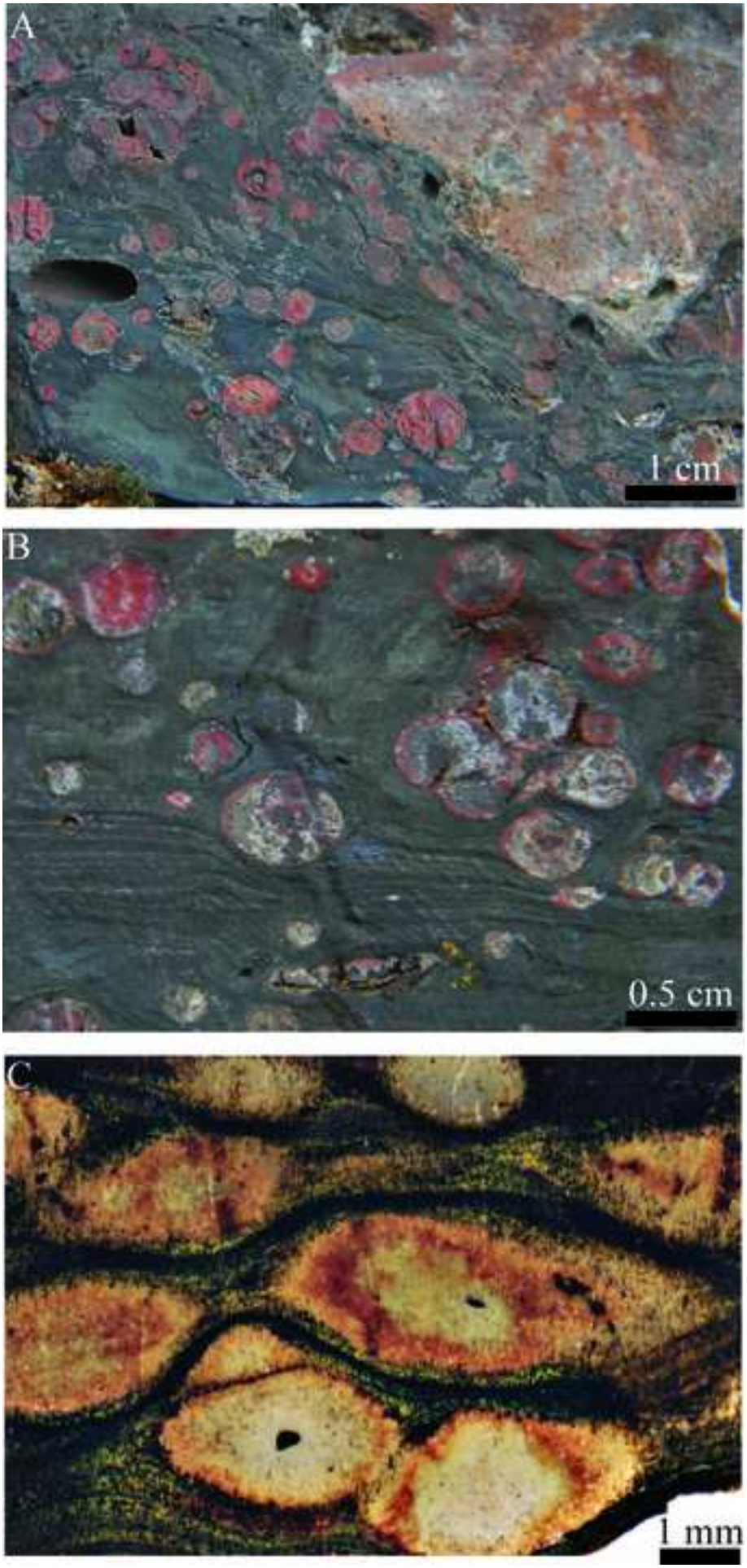

Figure 3

Click here to download high resolution image

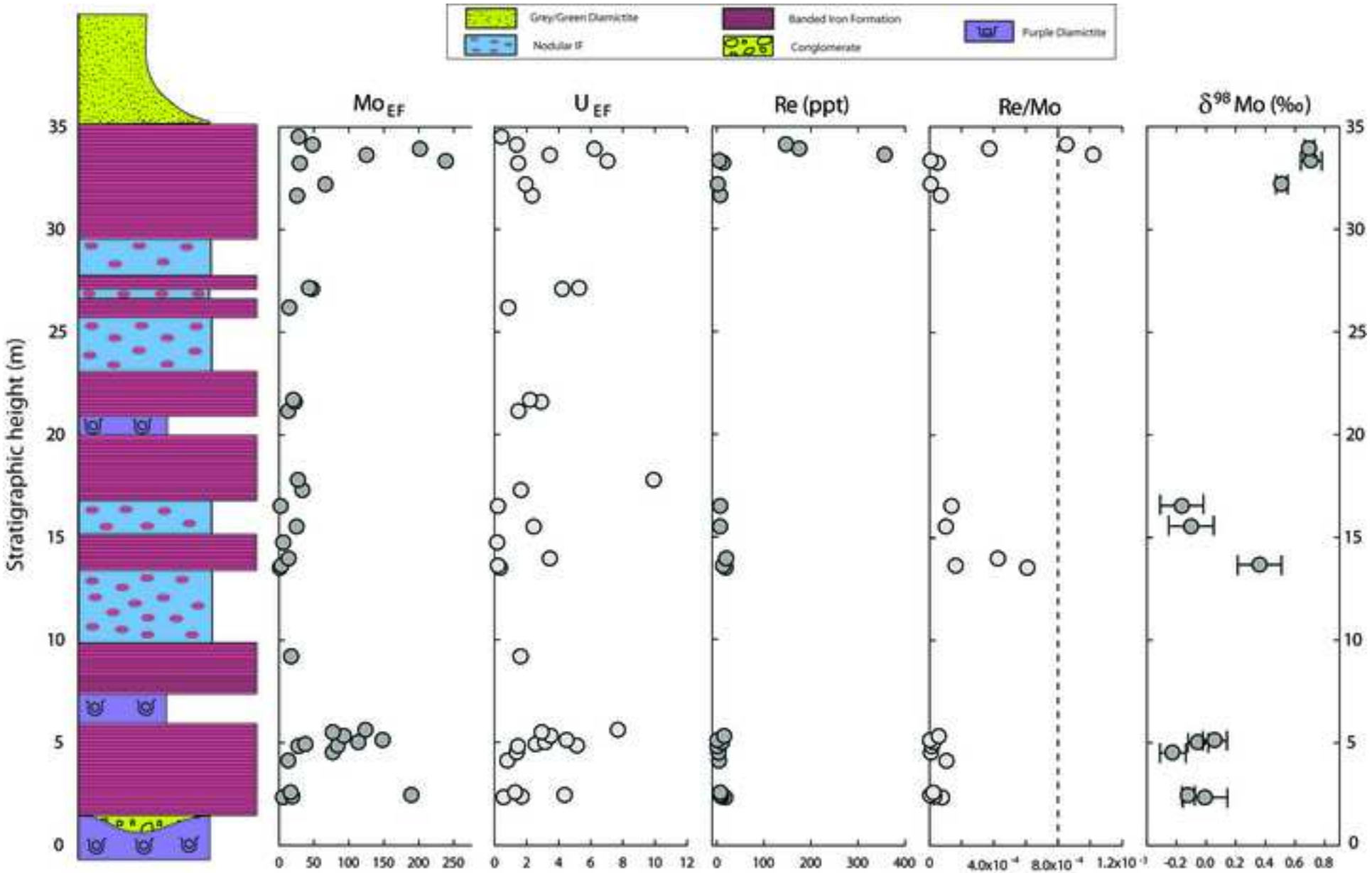

Figure 4

Click here to download high resolution image

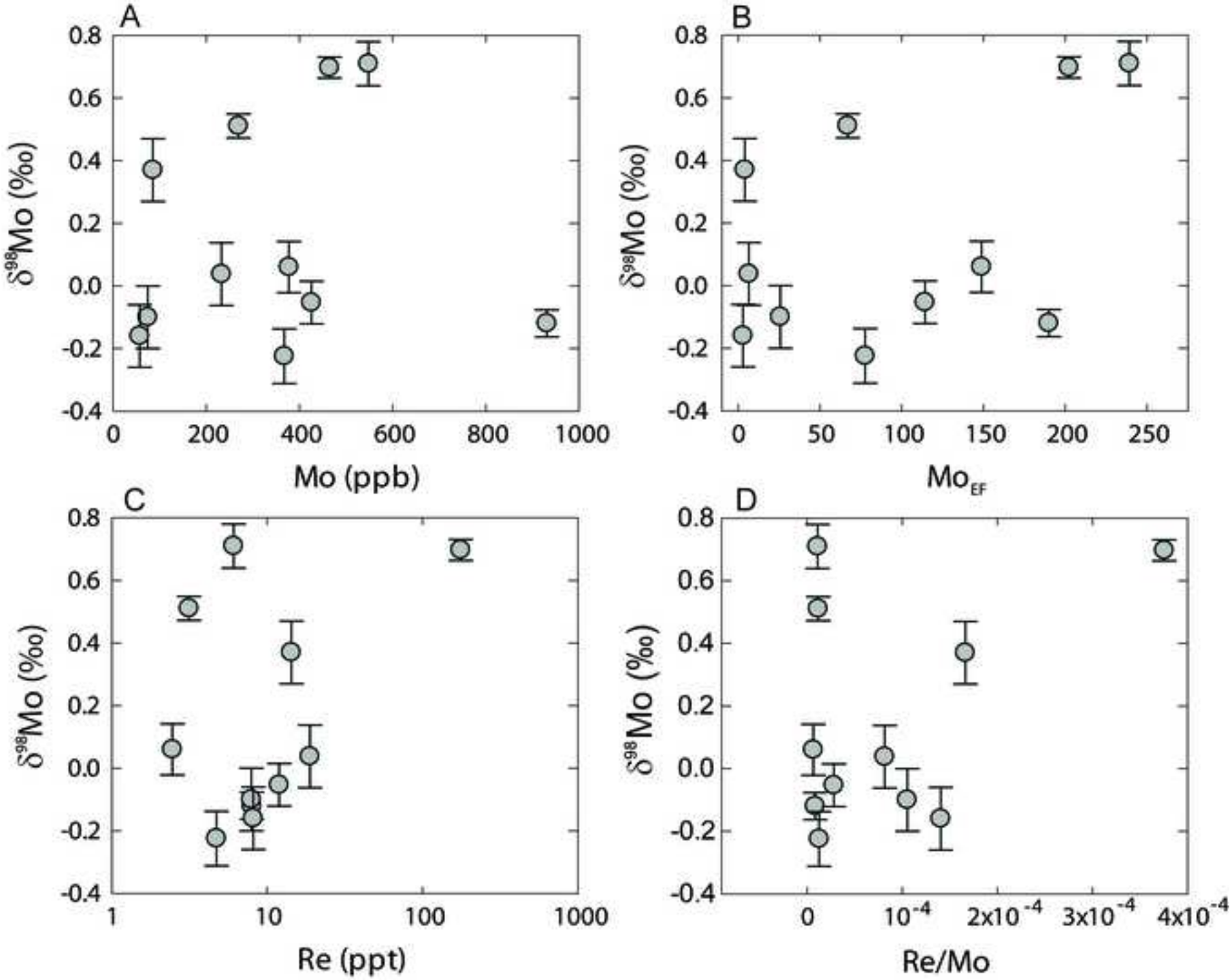

Table

Table 1: Results and errors

Strat height	Sample type	[1]Mo (ppb)	[1]U (ppb)	Re (ppt)	+	-	$^{1}Mo_{EF}$	$^{1}U_{EF}$	Re/Mo	$\delta^{98}Mo$	[3]2σ stdv
2.31	Jasper band	231.5	113.8	18.9	1.8	1.8	6.5	0.59	$8.15x10^{-5}$	-0.03	0.10*
2.35	Jasper band	335.7	158.8	11.1	1.7	1.7	19.7	1.72	$3.3x10^{-5}$		
2.42	Jasper band	933.7	117.4	8.0	1.2	1.2	189.9	4.40	$8.54x10^{-6}$	-0.12	0.04
2.55	Jasper band	304.8	126.0	8.4	1.5	1.5	17.2	1.31	$2.76x10^{-5}$		
4.1	Jasper band	51.9	16.9	5.6	1.1	1.1	13.9	0.83	$1.09x10^{-4}$		
4.5	Jasper band	372.0	36.7	4.7	1.5	1.5	77.6	1.41	$1.27x10^{-5}$	-0.22	0.09
4.8	Jasper band	130.4	36.9	2.3	1.0	1.0	28.6	1.49	$1.76x10^{-5}$		
5	Jasper band	426.3	64.6	12.0	1.5	1.5	114.2	3.19	$2.81x10^{-5}$	-0.05	0.07
5.1	Jasper band	378.8	62.5	2.5	1.2	1.2	148.8	4.52	$6.49x10^{-6}$	0.06	0.08
5.3	Jasper band	274.5	56.4	16.8	1.2	1.2	93.4	3.53	$6.12x10^{-5}$		
13.5	Jasper band	32.1	38.2	19.7	1.4	1.4	1.7	0.37	$6.13x10^{-4}$		
13.6	Jasper band	86.1	27.9	14.3	1.6	1.5	4.1	0.24	$1.66x10^{-4}$	0.37	0.10*
13.95	Jasper band	48.9	64.1	21.0	1.6	1.6	14.4	3.48	$4.29x10^{-4}$		
15.5	Jasper band	75.3	39.2	7.9	1.4	1.4	25.8	2.47	$1.05x10^{-4}$	-0.10	0.10*
16.5	Jasper band	58.0	25.3	8.1	1.0	1.0	3.0	0.24	$1.40x10^{-4}$	-0.16	0.10*
31.63	Jasper band	110.1	53.1	8.1	1.4	1.4	26.6	2.36	$7.36x10^{-5}$		
32.18	Jasper band	270.8	43.1	3.1	1.1	1.1	67.0	1.96	$1.16x10^{-5}$	0.51	0.04
33.21	Jasper band	265.9	71.3	14.4	1.6	1.6	30.5	1.51	$5.43x10^{-5}$		
33.32	Jasper band	551.4	88.5	6.1	1.3	1.3	239.2	7.07	$1.11x10^{-5}$	0.71	0.07
33.61	Jasper band	350.4	52.6	357.8	6.3	6.2	125.8	3.48	$1.02x10^{-3}$		
33.91	Jasper band	469.5	78.9	176.3	4.4	4.4	202.2	6.26	$3.75x10^{-4}$	0.70	0.03
34.11	Jasper band	173.0	27.2	147.9	3.8	3.8	48.8	1.41	$8.55x10^{-4}$		

Standards	Re (ppt)	+	-	$\delta^{98}Mo$	2σ stdv
Sco-1	1076	44	41		
BHVO-1	578	24	23		
[2]BCR-2	14390	2689	1970		
[4]NIST SRM 3134				0.25	0.09
[4]NIST SRM 610				0.31	0.09
[4]NIST SRM 612				0.29	0.10

[1]Data from Baldwin et al., 2012; samples without Re or δ98Mo analysis not included in table

[2]the error on BCR-2 was relatively high due to under-spiking

[3]Precision (2SD) under intermediate precision conditions of a single measurement (*, see text) or 2SD between 2 measurements

[4]NIST silicate glass standard reference materials, see Greber et al. (2012)